Full-Field Linear and Nonlinear Measurements using Continuous-Scan Laser Doppler Vibrometry and High Speed Three-Dimensional Digital Image Correlation

David A. Ehrhardt

Graduate Research Assistant, Ph.D. Candidate

dehrhardt@wisc.edu

&

Matthew S. Allen

Associate Professor

msallen@engr.wisc.edu

Department of Engineering Physics

University of Wisconsin-Madison

534 Engineering Research Building

1500 Engineering Drive

Madison, WI 53706

Shifei Yang

Development Specialist

shifeiy@gmail.com

Praxair Inc.

175 East Park Drive

Tonawanda, NY 14150

Timothy J. Beberniss

Aerospace Structures Engineer

Structural Sciences Centers, Aerospace Systems Directorate

Air Force Research Laboratory

Wright-Patterson Air Force Base, OH 45433

Abstract:

Spatially detailed dynamic measurements of thin, lightweight structures can be difficult to obtain due to the structure's low mass and complicated deformations under certain loading conditions. If traditional contacting sensors, such as accelerometers, strain gauges, displacement transducers, etc., are used, the total number of measurement locations available is limited by the weight added and the effect each sensor has on the local stiffness of the contact area. Other non-contacting sensors, such as Laser Doppler Vibrometers (LDV), laser triangulation sensors, proximity sensors, etc., do not affect the dynamics of a structure, but are limited to single point measurements. In contrast, a few recently developed non-contacting measurement techniques have been shown to be capable of simultaneously measuring the response over a wide measurement field. Two techniques are considered here: Continuous-Scan Laser Doppler Vibrometry (CSLDV) and high speed Three-Dimensional Digital Image Correlation (3D-DIC). With the use of these techniques, unprecedented measurement resolution can be achieved. In this work, the linear and nonlinear deformations of a clamped, nominally flat beam and plate under steady state sinusoidal loading will be measured using both techniques. In order to assess their relative merits, the linear natural frequencies, mode shapes, and nonlinear deformation shapes measured with each method are compared. Both measurement systems give comparable results in many cases, although 3D-DIC is more accurate for spatially complex deformations at large amplitudes and CSLDV is more accurate at low amplitudes and when the spatial deformation pattern is simpler.

Keywords: full-field measurement; continuous-scan laser Doppler vibrometry; high speed three dimensional digital image correlation; linear mode; nonlinear deformation

Nomenclature:

A_x	Amplitude of x laser position
A_y	Amplitude of y laser position
f	Frequency of input force
f_A	Scan frequency
f_x	x laser position frequency
f_y	y laser position frequency
N_x	Number of x laser position periods in Lissajous period
N_y	Number of y laser position periods in Lissajous period
T_A	Scan period
T_x	x laser position period
T_y	y laser position period
$x(t)$	x laser position

$y(t)$	y laser position
$\mathbf{z}(x,y,t)$	Stationary laser position in the time domain
$\mathbf{z}(x(t),y(t),t)$	Moving laser position in the time domain
$\mathbf{Z}(x,y,t)$	Stationary laser position in the frequency domain
$\mathbf{Z}(x(t),y(t),t)$	Moving laser position in the frequency domain

1. Introduction

The development of non contact full-field measurement techniques has received increased attention as the design of high-performance structures has advanced. Due to complex geometries and the lightweight nature of these structures, there is an increasing need for experimental techniques capable of measuring the response at a large number of degrees of freedom without modifying the structural response significantly. Techniques such as Continuous-Scan Laser Doppler Vibrometry (CSLDV) and high-speed Three-dimensional Digital Image Correlation (high-speed 3D-DIC) have been developed to meet this need. Both CSLDV and high-speed 3D-DIC are non-contact, non-destructive, and capable of accurately measuring the dynamic response at thousands of points across the surface of a structure. Both techniques are also capable of providing "real-time" measurements, but this has seen limited to no implementation for several reasons. In the case of 3D-DIC, significant computational power is needed to move and manipulate the thousands of image files sampled for each test. For CSLDV, real time measurement is theoretically feasible with the implementation of the harmonic power spectrum algorithm, but to the best of the author's knowledge this has never been done. For this work, these limitations are avoided by post-processing the data acquired with both methods.

CSLDV is an extension of traditional Laser Doppler Vibrometry (LDV), where the laser point, instead of dwelling at a fixed location, is continuously moving across a measurement surface. Therefore, obtaining vibration frequencies and deformation shapes from CSLDV signals is more challenging than from LDV signals since the moving measurement location requires the system to be treated as time-varying. Though this motion complicates the post-processing, the benefit provided by the continuously moving point is an increased measurement resolution with a drastically decreased measurement time when compared with traditional LDV. Several algorithms have been devised to determine a structure's deformation along the laser scan path. For example, Ewins et al. treated the operational deflection shape as a polynomial function of the moving laser position [1-6]. They showed that sideband harmonics appear in the measured spectrum, each separated by the scan frequency, and that the amplitudes of the sidebands can be used to determine the polynomial coefficients. Allen et al. later presented a lifting approach for impulse response measurements [7, 8]. The lifting approach breaks the CSLDV signal into sets of measurements from each location along the laser path. Hence, the lifted responses appear to be from a set of pseudo sensors attached to the structure, allowing conventional modal analysis routines to extract modal parameters from the

CSLDV measurements. However, this method works best when the laser scan frequency is high relative to the natural frequencies of interest, and for some structures this increase the measurement noise too much to be practical. Recently, algorithms based on Linear Time Periodic (LTP) system theory [9-14] were developed and used to derive input-output transfer function and power spectrum relationships from CSLDV measurements allowing the extraction of a structure's deformation from impulse, random, and sinusoidal excitations. When a structure is vibrating sinusoidally, many of the methods simplify significantly and in this paper the simplest method will be used based on Fourier analysis as was presented by Stanbridge, Martarelli, Ewins and Di Maio [1-6], and which is called the Fourier series expansion method in [7].

Displacements measured with 3D-DIC are challenging to obtain since each individual measurement point has to be matched in each image from each camera for the duration of the experiment. For high sample rates, this requires an additional step of post processing. Schmidt et al. [15] presented early work on the use of high-speed digital cameras to measure deformation and strain experienced by test articles under impact loadings. Tiwari et al. [16] used two high-speed CMOS cameras in a stereo-vision setup to measure the out of plane displacement of a plate subjected to a pulse input. Results compared favorably with work previously published and showed the capability of the 3D-DIC system in a high-speed application, although over a short time history. Niezrecki et al [17], Helfrick et al [18], and Warren et al [19] obtained mode shapes using 3D-DIC with different test articles using discrete measuring points. Niezrecki et al and Helfrick et al also combined accelerometers, vibrometers, and dynamic photogrammetry to compare results obtained with DIC analyzed at discrete measurement locations. Each technique provided complimentary results between all measurement techniques showing the capability of 3D-DIC, although 3D-DIC was not processed along the entire surface. Abanto-Bueno et al [20], Beberniss et al [21], and Ehrhardt et al [22] showed high speed 3D-DIC's capability to measure full-field dynamic deformations under large amplitude loading. Although, handling the large amount of data in conjunction with the image files can prove to be difficult.

In this investigation, CSLDV and high-speed 3D-DIC are used to measure the linear and nonlinear response of a clamped, nominally flat beam and plate. The linear response of each structure is measured when it is excited with a steady state sinusoid at selected natural frequencies using single-point mono-harmonic force appropriation. The nonlinear response of each structure is measured when it is excited with a steady state sinusoid at the first fundamental frequency of vibration in a nonlinear response regime. To process measurements from CSLDV, both the harmonic transfer functions and harmonic power spectra will be used to identify mode shapes of each structure when the response is linear and nonlinear, respectively. Displacements measured by 3D-DIC are processed using a commercial software Aramis [23] and its Real Time Sensor program [24].

2. Measurement Systems Theory

2.1 Continuous-scan Laser Doppler Vibrometry

A laser Doppler vibrometer (LDV) is a non-contact measurement technique that detects the Doppler frequency shift in a beam of laser light and converts it to the velocity component of the measurement point along the direction of the incident laser [25]. Continuous-scan laser Doppler vibrometry (CSLDV) extends the LDV measurement by moving the laser beam across the surface of a structure with a pre-defined pattern [1, 2]. CSLDV is capable of providing a dense array of measurements with a minimal increase in testing time. Scan patterns can range from simple lines and circles to complex Lissajous curves and trajectories. The selection of a pattern is not limited to periodic patterns only, as methods have been developed that are capable of measuring velocities if the pattern is aperiodic [4]. Methods developed for aperiodic scan patterns are limited to sinusoidal or impulse excitation which is applicable in this work; however, an aperiodic scan pattern would cover the entire surface of the plate after sufficient time. Therefore, the whole surface would need to be coated with a retro-reflective coating to obtain the best results, which would not leave room to apply the speckle patterns that are needed for 3D-DIC. Instead, periodic 1-D line and 2-D Lissajous curve patterns were used in this work. Another advantage of this approach is that the observed mode shape becomes a periodic function of time [7, 13] and hence the deformation shape doesn't need to be approximated with a polynomial in the spatial coordinates as is typically done in [1-5]. The selected periodic patterns are scanned across a surface using a single point fiber optic LDV and external mirrors, as shown in Fig. 1. Further discussion of the physical setup is presented in Sec. 2.3.

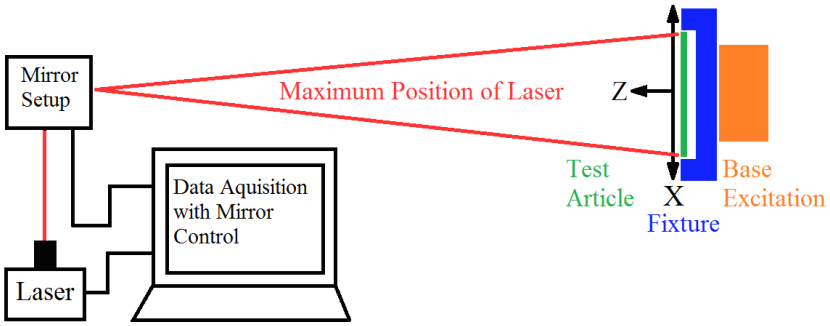

Figure 1: CSLDV System Diagram. The laser beam was redirect by a pair of rotating mirrors.

The implementation of a time-periodic CSLDV scan pattern couples the motion of the measurement point with the deformation of the structure. Therefore, additional processing is required to separate the motion from the structural deformation in order to reconstruct the vibration shapes. Consider the measurement of vibration along a single axis with a

single point sensor. The measured response $\mathbf{z}(x,y,t)$ of a linear time invariant (LTI) structure subjected to a single frequency force input is harmonic at the same frequency, f, but with a different phase and amplitude at each point, so it can be written as follows.

$$\mathbf{z}(x,y,t) = \mathrm{Re}(\mathbf{Z}(x,y)e^{i2\pi * f * t} \tag{1}$$

Here x and y represent the sensor position on the surface. If CSLDV is used with a periodic scan pattern, the measured response becomes time periodic, $\mathbf{z} = \mathbf{z}(x(t),y(t),t)$, as follows

$$\mathbf{z}(x(t),y(t),t) = \mathrm{Re}(\mathbf{Z}(x(t),y(t))e^{i2\pi * f * t} \tag{2}$$

where the x- and y-coordinates change in time based on the predefined periodic motion

$$\begin{aligned} x(t) &= A_x \cos(2\pi f_x t) \\ y(t) &= A_y \sin(2\pi f_y t) \end{aligned} \tag{3}$$

For the Lissajous patterns used here, the period T_A of the scan pattern is determined by both x- and y- scan frequency, as defined in Eqn. (3), and modifying the values for f_x and f_y changes the density of the pattern across the scan.

$$T_A = \frac{1}{f_A} = N_x * T_x = N_y * T_y = N_x * \left(\frac{1}{f_x}\right) = N_y * \left(\frac{1}{f_y}\right) \tag{4}$$

As the amplitude $\mathbf{Z}(x(t),y(t))$ is periodic, it can be represented with a Fourier Series as shown below.

$$\mathbf{Z}\big(x(t),y(t)\big) = \mathbf{Z}(t) = \mathbf{Z}\big(t+T_A\big) = \frac{1}{2}\sum_{n=-\infty}^{\infty}\mathbf{Z}_n e^{in2\pi * f_A t} \tag{5}$$

The periodic motion of the laser couples with the structural deformation inducing a periodicity in the measurement. Inserting the Fourier series description of the deformation shape into Eqn. (2), one obtains the Fourier description of the CSLDV signal shown in Eqn. 6; the measured response using CSLDV includes motion at the input frequency and an infinite number of harmonics separated by the scan frequency f_A. Since the laser scan path is known, the deformation of the structure can be recovered by measuring the amplitudes of all of these harmonics, following a procedure similar to that which was presented in [13].

$$\mathbf{z}\big(x(t),y(t),t\big) = \mathbf{Z}\big(x(t),y(t)\big)e^{i2\pi ft} = \frac{1}{2}\sum_{n=-\infty}^{\infty}\mathbf{Z}_n e^{i2\pi(f+nf_A)t} \tag{6}$$

2.2 High Speed 3 Dimension Digital Image Correlation

To accurately measure 3D displacements with DIC, a setup using two cameras is used to image the test article as it deforms. As shown in Fig. 2, the two cameras are placed at a specific distance along the Z-axis from the test article to allow the surface to be captured simultaneously in each camera and establish a field of view. A pan angle, Θ_p, is specified based on a desired depth of view or range of out-of-plane displacements expected [23].

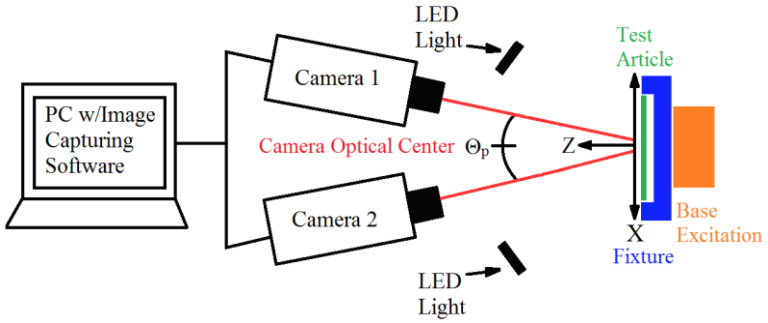

Figure 2: 3D-DIC System Diagram. The 3D-DIC system diagram shows Camera 1 (left camera) and Camera 2 (right camera) set to a specified pan angle, Θ_p.

Once the stereo camera setup is assembled and fixed, principles of triangulation are used to establish each camera's position in reference to the global experimental coordinate system as defined by:

$$\begin{bmatrix} x_{Camera} \\ y_{Camera} \\ z_{Camera} \end{bmatrix} = \mathbf{R} \begin{bmatrix} x_{Global} \\ y_{Global} \\ z_{Global} \end{bmatrix} + \mathbf{T} \tag{7}$$

Where **R** is the rotation matrix and **T** is the translation matrix for the coordinate system transformation. Additionally, lens distortion and variations between the sensor of the camera and the final images can be corrected through a bundle adjustment [26]. The coordinate system transformation matrix is established through the use of images of a rigid known pattern or calibration panel. With this calibration, the accuracy of the coordinate transformation matrix is not limited to the pixel size of the imaged surface of the test specimen, but instead can be interpolated on the sub pixel level (i.e. calibration deviation of about 0.01 to 0.04 pixels are typical [23]). Once the calibration of the 3D-DIC system is established, images of the fully deformable structure can be analyzed to obtain displacements. To achieve a sub pixel accuracy in the determination of displacements, the surface of the structure is divided into areas of pixels or subsets. Each subset in turn is fit with a surface following the form of:

$$\begin{bmatrix} A \\ B \end{bmatrix} = \begin{bmatrix} x \\ y \end{bmatrix} + \begin{bmatrix} a \\ b \end{bmatrix} + \begin{bmatrix} \partial a/\partial x & \partial a/\partial y \\ \partial b/\partial x & \partial b/\partial y \end{bmatrix} \begin{bmatrix} \Delta x \\ \Delta y \end{bmatrix} + \begin{bmatrix} \partial^2 a/\partial x \partial y \\ \partial^2 b/\partial x \partial y \end{bmatrix} \Delta x \Delta y + \begin{bmatrix} \partial^2 a/\partial x^2 & \partial^2 a/\partial y^2 \\ \partial^2 b/\partial x^2 & \partial^2 b/\partial y^2 \end{bmatrix} \begin{bmatrix} (\Delta x)^2 \\ (\Delta y)^2 \end{bmatrix} \quad (8)$$

Where A and B are the final deformed coordinates of the center of the subset, x and y are the original coordinates, a and b are the rigid translation of the subset and the three remaining matrices correspond to an affine, irregular, and quadratic deformation of the subset, respectively. Using a correlation algorithm, each subset is matched through each imaged deformation providing out of plane displacement accuracies on the order of 0.03 pixels (or 10 μm for the 300mm field-of-view used in this work) depending on the correlation algorithm used. In-plane deformations are measured with a greater accuracy when compared with purely out-of-plane deformations since in-plane deformations are less reliant on the higher order fit of the subset surface. Prior to testing, a high-contrast random gray-scale pattern is applied to the measurement surface so the defined subsets can be uniquely and accurately fit. As detailed in [26], triangulation of the subset matching is used to determine the coordinate value of each measurement point.

3. Experimental Setup

The physical experimental setup is shown in Fig. 3. In this setup, there are four main systems: 1) exciter/ controller, 2) static 3D-DIC system, 3) dynamic 3D-DIC system, and 4) the CSLDV system.

1) Excitation was provided by two separate exciters, both controlled in an open-loop using a Wavetek Variable Phase Synthesizer. The low amplitude excitation was provided by an Electro Corporation 2030 PHT magnetic pickup which was given a high voltage input from a Piezo Amplifier. This induces a localized magnetic field providing a near single point input force to ferrous materials. If non-ferrous materials are used or more force is required, a thin magnetic metal dot can be added to a structure. The force exerted by the magnetic pickup was measured using a force transducer mounted between a solid base and the magnetic pickup providing measurement of the reaction force with the base. Large amplitude excitation was provided by shaking the base of the structure's clamping fixture which was mounted on a 5000N MB dynamics shaker. However, this type of excitation provides uniform inertial loading and limits the ability to examine asymmetric motion of the structure. The voltage input to the exciter was measured as well as the input force for the magnetic driver and the base acceleration for the shaker.

2) The static 3D-DIC system consists of two Prosilica GT2750 CCD cameras with a full resolution of 2750 x 2200 pixels with a maximum frame rate of 20 fps. For this experimental setup, full resolution images were used since the camera memory was not a limiting factor. The static system uses 18mm lenses and is positioned at a standoff distance of 580mm

with a camera angle of 26 degrees. All static displacements were determined using a commercial 3D-DIC software Aramis [17] using subsets of 31x31 pixels with a 13 pixel overlap across the entire surface of the plate. A 250mm x 200mm calibration panel was used to establish the measurement volume and lead to a calibration deviation of 0.032 pixels for this camera resolution or 0.004 mm for this field of view.

3) The dynamic 3D-DIC system includes two Photron, high speed 12-bit CMOS cameras (model Fastcam SA5 775K-M3K). Each camera has 32GB of memory onboard with a maximum resolution of 1024×1024 pixels. For each experimental setup, image size was adjusted to fit as much of the structure in the frame of both cameras resulting in a field of view of approximately 300 x 300mm. The dynamic system uses 85mm lenses at a standoff distance of 1370mm with a camera angle of 24.4 degrees. All dynamic displacements were determined using a software extension of Aramis called IVIEW Real Time Sensor [24] using subsets of 15x15 pixels. In order to minimize the heat generated and remove the electrical noise produced by the lighting systems that are typically used in high-speed DIC systems, two 305×305 LED light panels were used. The cameras and the data acquisition system were simultaneously started using an external TTL trigger, with the cameras capturing images at 5000 frames per second. Measurement points were selected to avoid the retro-reflective tape, so there is no overlap of measurements between CSLDV and 3D-DIC. A 250mm x 200mm calibration panel was used to establish the measurement volume and lead to a calibration deviation of 0.02 pixels for this camera resolution or 0.007 mm for this field of view.

4) The continuous-scan mechanism was built using a Polytec OFV-552 fiber optic laser vibrometer with a sensitivity of 125 mm/s/V and the same external mirror system that was used in [8]. The mirrors were positioned at a stand off distance of 2.4m, which was selected to minimize the scan angle, which was a maximum of 7.3 degrees in x-direction and 5.4 degrees in y-direction for both setups, and yet keep the laser close enough to maintain a high quality signal. The external mirror system consisted of two galvanometer scanners in open-loop control; each scanner had a position detector that measured the instantaneous rotation angle, allowing precise and accurate control and measurement of the laser position. The control and data acquisition system was built using a National Instruments PXI system. A LabVIEW program was developed to integrate several features including the function generator, data acquisition, and signal processing. The line and Lissajous patterns used for this investigation have a x-direction scan frequency of 3 Hz and the y-direction scan frequency of 4 Hz. Data was collected at each steady state response level with a sampling frequency of 10,240Hz for 2 minutes.

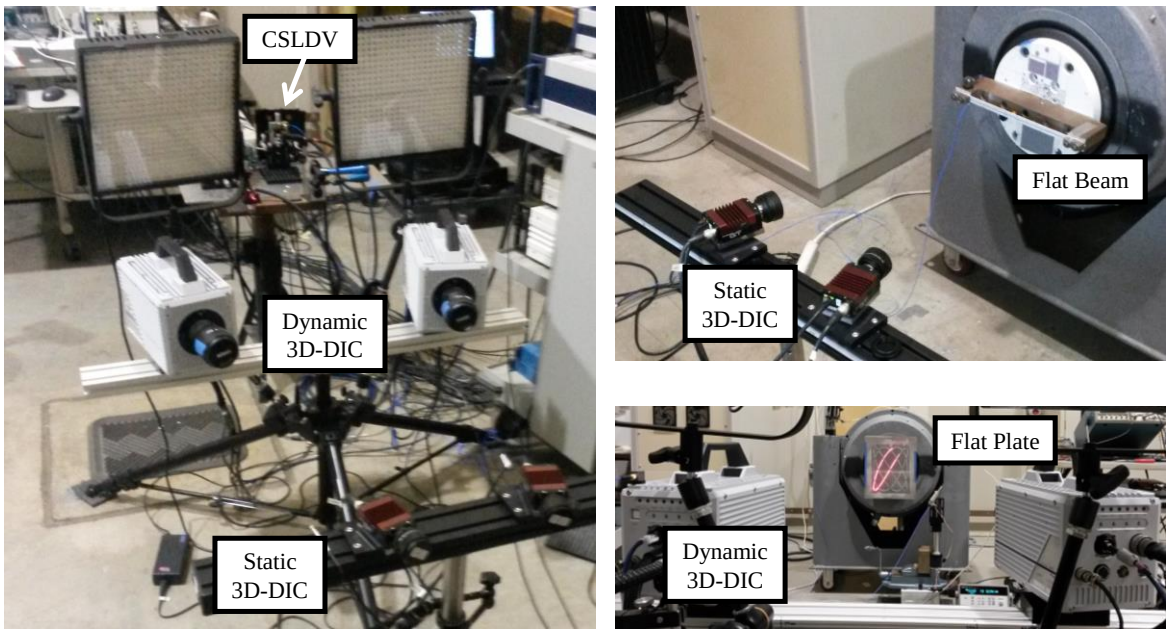

Figure 3: Experimental Setup.

4. Flat Clamped-Clamped Beam

The first structure under test for this investigation is a precision-machined feeler gauge made from high-carbon, spring-steel in a clamped-clamped configuration, as was previously studied in [27]. This beam is selected because the machining tolerance for the thickness is as precise as possible so any error in the thickness would be overpowered by boundary conditions and initial geometry variations. The beam is assumed to be flat and has an effective length of 228.6mm, a nominal width of 12.7mm, and a thickness of 0.762mm. All presented dimensions are nominal and subject to variation from clamping and from the machining process to obtain the desired thickness. Prior to clamping, the beam was prepared for three dimensional digital image correlation (3D-DIC) and continuous-scan laser Doppler vibrometry (CSLDV) as discussed in [28] and shown in Fig. 4a. Locations of the initial laser Doppler vibrometry (LDV) positions are also shown at the center of the beam and 12mm to the left of the center measurement. The clamping force was provided by the two 6.35-28 UNF-2B bolts tightened to 90 in-lbs. Before and after clamping the beam in the fixture, static 3D-DIC was used to measure the initial curvature of the clamped beam and the result is shown in Fig. 4b. It is interesting to note that although the beam is assumed to be nominally flat, before and after clamping the beam has an initial deflection of 4% and 0.01% of the beam thickness, which is not obvious during clamping. The coordinate system used for the 3D-DIC setup was defined using the edges of the clamps, which are visible in the images. This change of initial curvature has little effect on the linear results, but could change the characteristic nonlinearity of the beam (e.g. softening to hardening effect). Additionally, single-input single-

output modal hammer tests were performed throughout testing on the beam to check the consistency of the final clamped beam. Results from these hammer tests showed a 0.7% variation in the first natural frequency of the final clamped beam, which can be expected due to a small amount of slipping or temperature variation in the room.

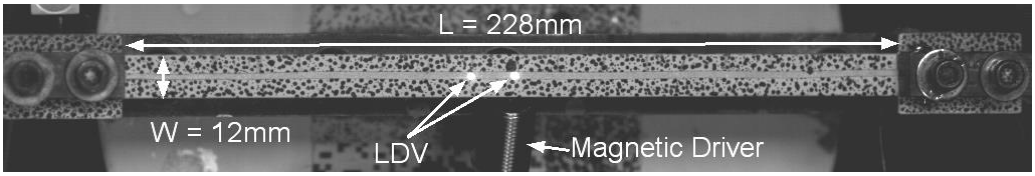

(a)

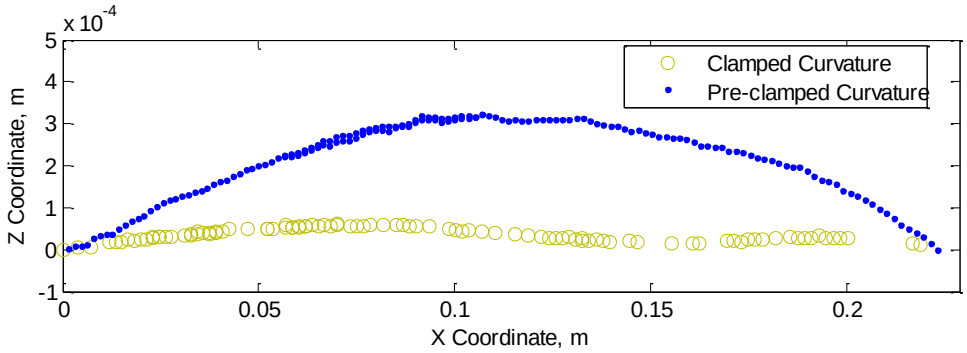

(b)

Figure 4: Beam Specimen. a) Final clamped-clamped configuration, b) Initial clamping deformation

Table 1: Modal Comparison

Mode	f_n AVG Modal Hammer Test, Hz	% Change between Pre- and Post- Experiment Modal Hammer Tests	f_n CSLDV, Hz	% Error between CSLDV and Hammer Test	f_n DIC, Hz	% Error between DIC and Hammer Test	MAC
1	71.75	-0.70	71.24	-0.7112	71.30	-0.6269	0.9995
2	204.35	-0.49	204.33	-0.0117	204.50	0.0747	0.9981
3	411.45	-0.12	411.05	-0.0972	411.39	-0.0134	0.6572

In order to measure the deformation of the beam with one measurement system setup, an understanding of the limitations of each measurement system is needed. For instance, measurements with 3D-DIC become contaminated with noise at small deformations as a result of sensor limitations of the imaged surface area. Also, measurements with CSLDV can become contaminated with noise at small deformations due to the added speckle noise from the moving laser point. Additionally, the cameras used for 3D-DIC need to be able to 'see' the deforming surface to make a measurement possible which limits the amount of deformation the structure can undergo. Also, the laser used for CSLDV will disperse more when the structure undergoes large deformation also limiting the amount of deformation the structure can undergo. Therefore,

special consideration is needed when setting the field- and depth-of-view for 3D-DIC and when selecting the scanning frequency and standoff distance for CSLDV so both systems can simultaneously measure the deformation of the structure when undergoing small or large deformations. Alternatively, 3D-DIC and CSLDV measurement setups can be chosen so one can measure smaller deformations and one can measure larger deformation with an overlap where both systems can measure the deformation of the structure. For this experimental setup, the latter case is true and deformations on the order of 0.02 mm are the low end for 3D-DIC, where CSLDV can measure down to 0.0002 mm. No upper limit is identified for the structures investigated since the structures investigated would have been damaged at this high level of deformation. To find the area of measurement overlap the beam was driven at the largest force that allowed a near linear response in the beam. This force was determined by incrementally increasing the input force level while monitoring damping. When damping increased a measurable amount, the force was decreased to the previous forcing level. The maximum resulting response was 62% of the beam thickness which is a weakly nonlinear level.

4.1 Linear Beam Response Comparison

The clamped beam was driven using mono-harmonic sinusoidal forcing at each of the first three natural frequencies identified with the single-input single-output modal hammer tests. The beam's steady state response under these forcing conditions was measured using high-speed 3D-DIC and CSLDV. Fig. 5 (a) shows an example of the response spectrum from 3D-DIC measured at the center of the beam when it is forced at the first natural frequency. The fast Fourier transform results are take from 1 second of data captured at 5000 frames per second. Only the out-of-plane displacements are shown for 3D-DIC since the axial and transverse displacements are in the noise of the measurement. As expected, a single harmonic is seen in the response at 71.3Hz, which is the forcing frequency. Higher harmonics are also observed at 137.4Hz and 140.9Hz, which correspond to the camera fan noise, and at 142.6Hz which corresponds to a second harmonic in the response of the beam. Fig. 5 (b) shows an example of the response spectrum from CSLDV measured as the laser scans the beam's surface. In addition to the primary harmonic of the response at 71.44Hz, several side-bands are observed in the response spectrum each separated by the scanning frequency of 3Hz. As previously discussed, an infinite number of sidebands are expected for CSLDV, but Fig. 5(b) shows sideband harmonics higher than the 6th order are buried in the noise. So, no harmonics above the 6th order were used. Hence, only the Fourier coefficients for harmonics of n = -6:6 were used to construct the mode shape along the laser path. Similarly, the second and third bending mode shapes were reconstructed using the Fourier coefficients that stood out above the noise floor, which ended up being harmonics n=-10...10 and n=-15...15, respectively. Higher harmonics are also observed around 142.9Hz corresponding to the second harmonic of the beam response.

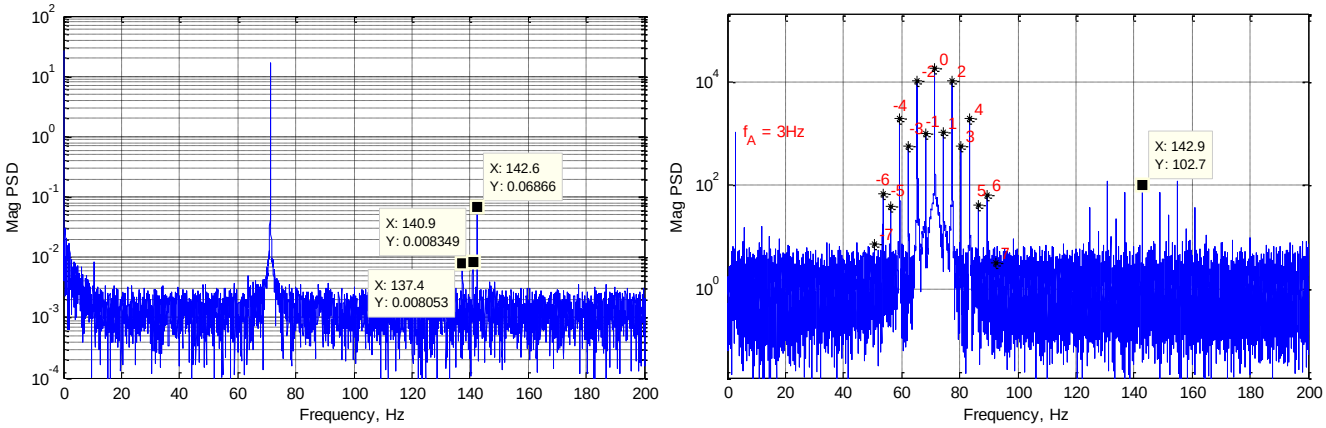

Figure 5: Linear Response Spectrum Comparison. (Left) 3D-DIC and (Right) CSLDV

Figure 6 compares the mode shapes obtained by CSLDV and 3D-DIC when exciting near each of the three resonance frequencies. Figure 6(a) contains the mode shape at 71.3Hz and shows the difference between the mode shapes measured with CSLDV and the measurement points obtained with high-speed 3D-DIC. Similarly, Figure 6(b) and 6(c) show the mode shapes at 205.5Hz and 411.4Hz. The MAC values between DIC and the CSLDV shapes are shown in table 1 along with the frequency errors previously discussed. It is noted that MAC values for modes 1 and 2 are above 0.99 showing excellent correlation between CSLDV and high-speed 3D-DIC; for the third mode at 411 Hz the maximum displacement was only 0.21mm measured at 411.4Hz, high-speed 3D-DIC begins to exhibit larger errors in the mode shape, which is shown in Figure 6(c), leading to a MAC value of 0.6572.

Additionally an asymmetry is seen in the mode shapes of modes 2 and 3 which is believed a result of asymmetry of the boundary conditions or the initial curvature in the beam. Both measurement methods capture the asymmetry in mode 2, but the asymmetry for mode 3 is apparently not detected as accurately in CSLDV as with 3D-DIC. The accuracy of each method is difficult to ascertain for the measurement of mode 3 since 3D-DIC begins to lose measurement resolution and higher harmonics from CSLDV measurements are buried in the noise of the laser signal. In either case, the asymmetry would be undetectable unless the dynamic response is observed with the large number of measurement points.

It is also important to note that while the smooth nature of the CSLDV mode shapes seems to suggest that they are infallible, they are in fact an approximation of the true mode shapes obtained by expanding them in a Fourier series of the time-varying scan pattern. The accuracy of the reconstructed mode shape depends on the number of harmonics included in the Fourier series approximation. As mentioned previously, thirteen clearly dominant harmonics (i.e. n=-6...6) were observed

for the first mode. The neglected harmonics were at least a few orders of magnitude smaller than the dominant ones, so one would be inclined to have high confidence in that shape. The harmonics n = -8...8 were also used to reconstruct the first bending mode shape, the results was only 0.068% different from the shape that was shown which used harmonics n = -6...6. Furthermore, because the laser is scanning along a line with CSLDV, when the measurements are noisy, the mode shapes measured on the forward and backward parts of the sweep tend to differ giving an indication of the error. Here, the forward and backward sweeps overlay completely suggesting that the shapes shown are quite accurate.

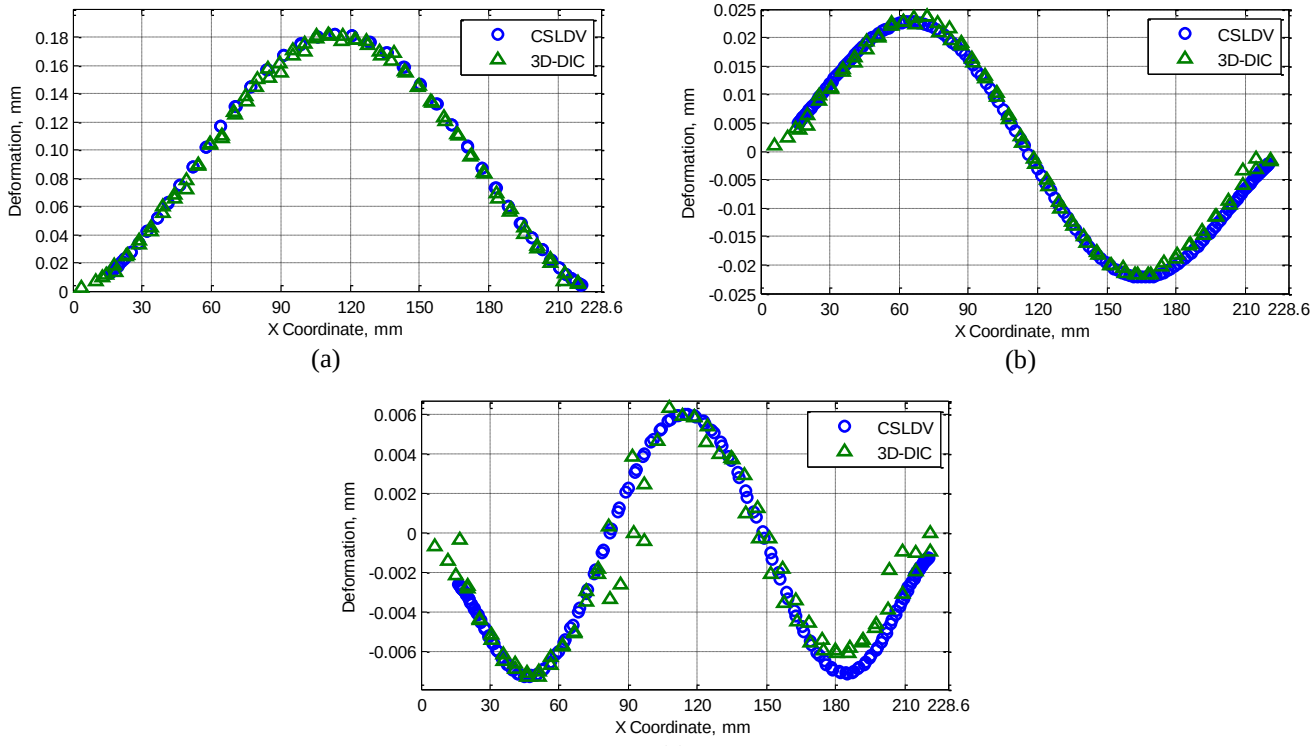

Figure 6: Modes shapes from Steady State Excitation. a) Mode 1 at 71.3Hz, b) Mode 2 at 204.5Hz, and c) Mode 3 at 411.4Hz.

4.2 Nonlinear Beam Response Comparison

As a structure is pushed towards the nonlinear regime, a single harmonic input force results in a multi-harmonic response. Figure **7** shows the resulting nonlinear response spectrum for 3D-DIC and CSLDV. For 3D-DIC, 10 harmonics of the forcing frequency can be easily identified in the measured response. The additional harmonics seen in the 3D-DIC response near 140 Hz can be attributed to previously identified fan noise from the camera cooling fans. As discussed later, the deformation shape at all 10 harmonics cannot be fully visualized for 3D-DIC due to variations in the measurement across the surface, especially when the response has small displacement. For CSLDV, the scanning laser permits the identification of 7 harmonics of the forcing frequency in the measured response. Due to increased laser dispersion from the 3Hz motion of the laser the noise floor is increased reducing the ability to identify all 10 of the fundamental harmonic components. Also, at

higher harmonics, the deformation shape of the beam becomes more complex, so more side band harmonics are needed to reconstruct the deformation shape of the beam. However, the added noise of the scanning laser reduces the ability to identify side band harmonics in the measured response.

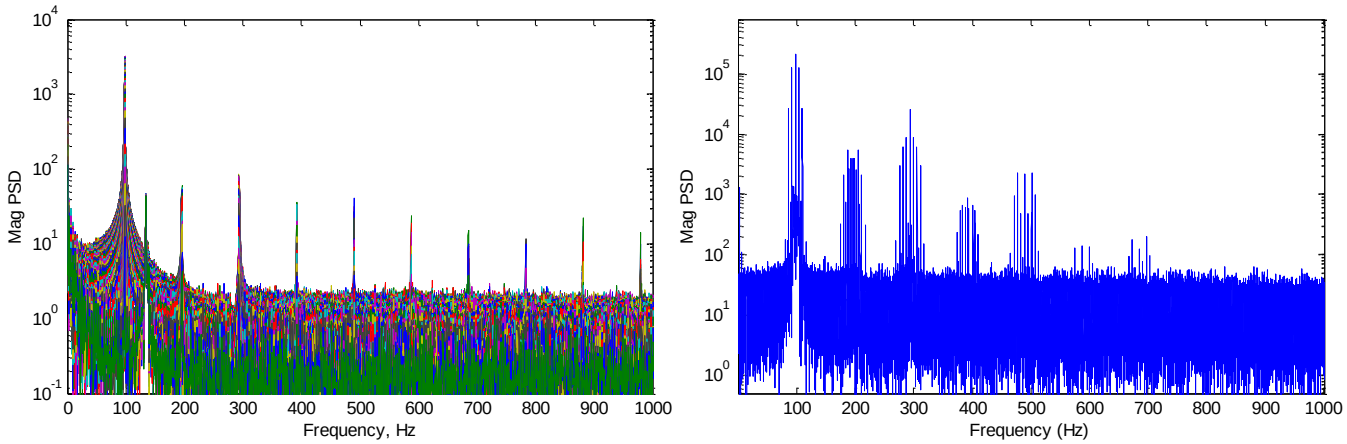

Figure 7: Nonlinear Beam Response Spectrum Comparison. (Left) 3D-DIC and (Right) CSLDV

Full-field measurements of a deforming structure, such as this beam, are especially beneficial for nonlinear deformations since the spatial deformation of the beam can be identified at each harmonic. These measurements can then in turn be used in model updating to identify nonlinear coupling in the beam's modes. Figure 8a-e shows the deformation patterns along the beam for selected harmonics. Figure 8a shows the first harmonic of the response, or the fundamental harmonic, which resembles the first linear mode of a flat beam as expected. There is a small shift in the deformation of the first harmonic made with CSLDV and 3D-DIC, but both systems correctly show a zero deformation at the clamps of the beam. Each measurement system establishes an independent reference coordinate system, and this shift corresponds to a 6 degree rotation about the y-axis of one of the measurement systems relative to the other. This is certainly within the uncertainty in the alignment of the two measurement systems. Figure 8b shows the second harmonic of the response, which resembles the second linear mode of a flat beam, with a factor of two difference between the peak deformations of each lobe. The maximum deformation of this harmonic is 0.013mm, which apparently causes 3D-DIC to begin to lose measurement resolution in this and subsequent harmonics. Figure 8c shows the third harmonic of the response, where the deformation resembles a superposition of mode 1 and mode 3 of the beam. Again, 3D-DIC appears to lose measurement resolution at these small displacements, but the basic deformation shape is still captured. Figure 8d shows the fourth harmonic of the response which does not resemble a linear mode of vibration. At this harmonic 3D-DIC completely loses ability to measure the beam deformation and CSLDV begins to loose accuracy, as is manifest in the difference between the shapes measured in the forward and backward sweeps. Figure 8e shows the fifth harmonic of the response which occurs at a higher level of

deformation than the fourth. Therefore, 3D-DIC is able to capture the response but the measurement resolution is still reduced. The amplitude of this harmonic is higher than the fourth, but the deformation pattern is more complex, so CSLDV also shows variation in the forward and backward sweeps for this mode. For the low levels of deformation presented here, CSLDV outperforms 3D-DIC in capturing these spatial deformation shapes.

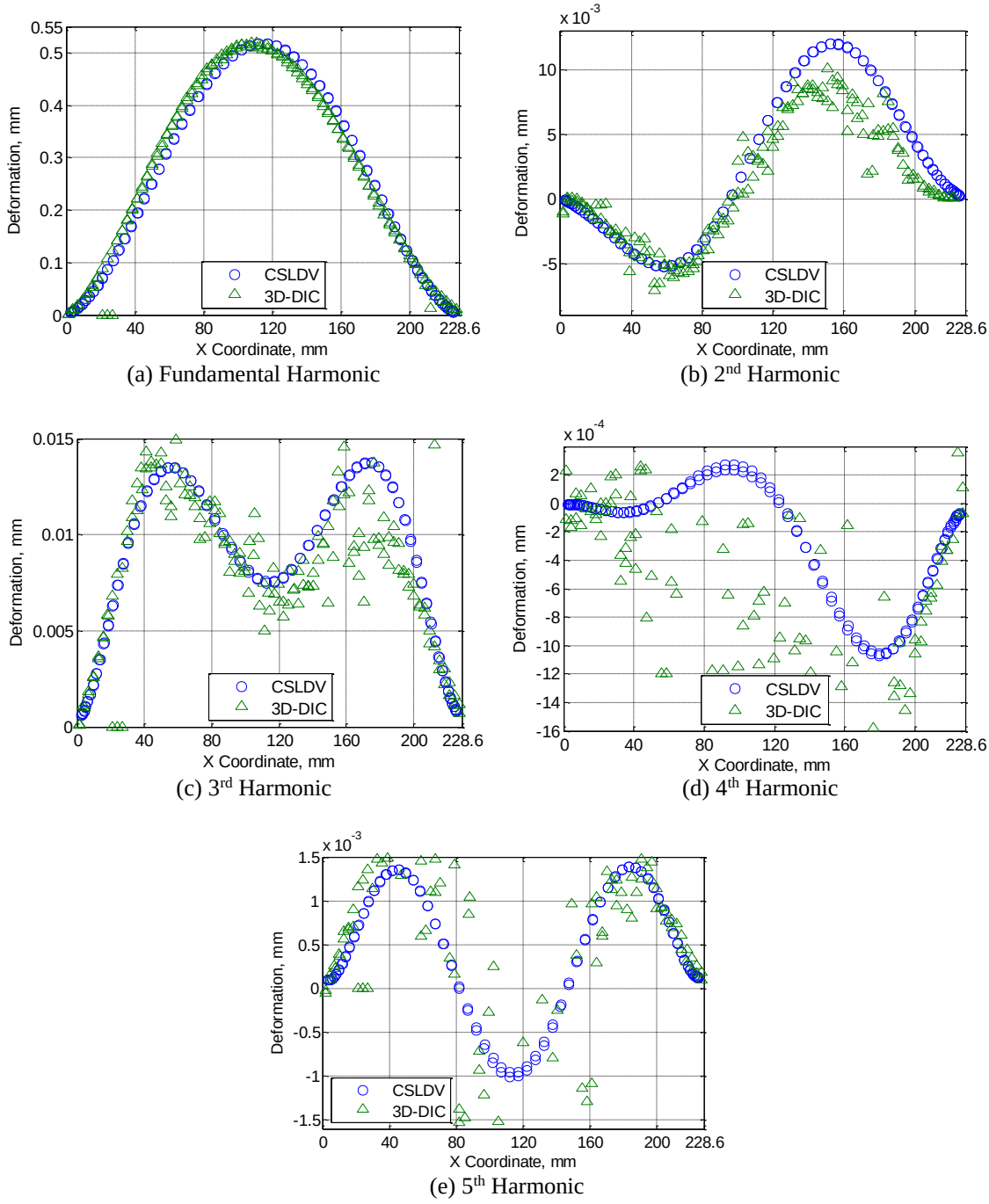

(a) Fundamental Harmonic

(b) 2nd Harmonic

(c) 3rd Harmonic

(d) 4th Harmonic

(e) 5th Harmonic

Figure 8: Deformation pattern for each harmonic in the response of the beam. The legend shows the frequency from which these harmonics were extracted and the peak deformation amplitude in each shape.

5. Flat Clamped-Clamped Plate

The second structure under test for this investigation is a nominally flat clamped aluminum plate. The tested plate had an effective length of 177mm, an effective width of 228mm, and a thickness of 0.5mm. The plate was then clamped between two mounting frames with adhesive as further described in [29]. After being fixed between the mounting frames, the plate was painted with a white base coat, and a speckle pattern with an average diameter of 5 pixels was applied using a marker and spray paint to increase the imaged surface texture and improve tracking for the static and dynamic 3D-DIC systems. Once the plate had dried, a pattern of retro-reflective tape cut from a printed Lissajous stencil was added to increase feedback to the CSLDV laser while not covering the rest of the plate so that 3D-DIC could be used in those areas. The final prepared plate is shown in the clamping fixture in Figure **9**a. For an accurate description of the initial conditions of the plate, static 3D-DIC images were captured after the plate was fully clamped. An initial deflection of 0.613 mm near the center of the plate was measured, as shown in Figure **9**b, where the color bar corresponds to the defined z-coordinate. One can see that the retro-reflective tape and the edge of the mounting frame have a negative effect on the ability of 3D-DIC to compute the static coordinates at certain positions, but the measurement density is high in other regions so it is not difficult to interpolate over the anomalies that these introduce. The final step of preparation was the addition of a 6mm steel disk to the back of the aluminum plate to allow input force from a magnetic driver, discussed in the next section. The location of this disk is shown in Figure **9**a.

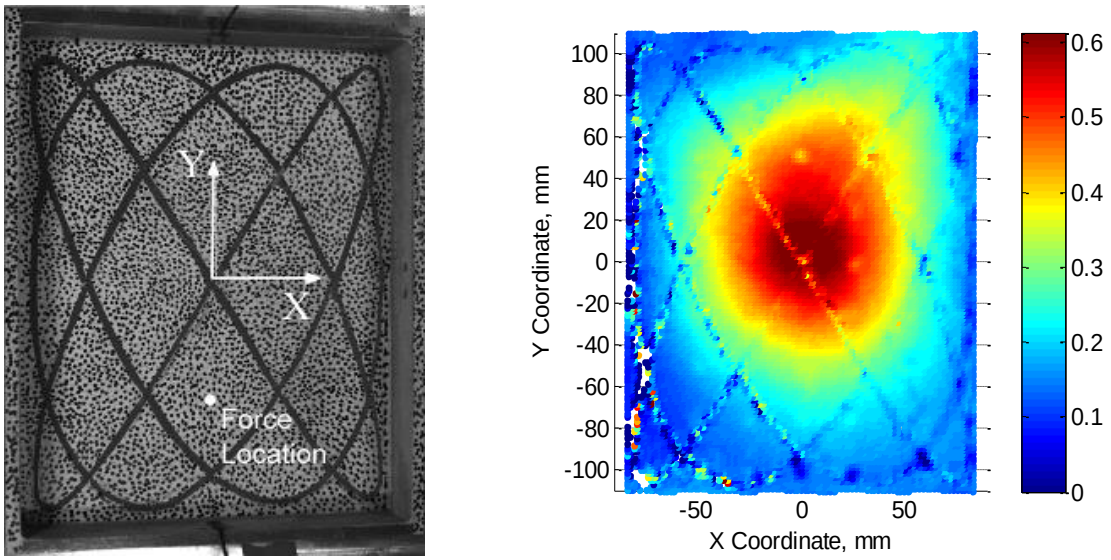

(a) (b)

Figure 9: Images of Rectangular Plate: a) Final prepared surface, b) Measured initial curvature. The color bar gives the z coordinate in mm.

Table 2: Plate linear frequencies

Mode	f_n AVG Modal Hammer Test, Hz	% Change between Pre- and Post- Experiment Modal Hammer Tests	f_n CSLDV, Hz	% Error between CSLDV and Hammer	f_n DIC, Hz	% Error between DIC and Hammer
1	106.5	0.65	106.9	0.3756	106.7	0.1878
4	276.5	0.43	275	-0.5425	275.1	-0.5063

5.1 Linear Plate Response Comparison

Force appropriation was used to drive the plate at the first and fourth natural frequencies and the steady state response was measured using both CSLDV and high-speed 3D-DIC. Figure 10 shows an example of the spectrum from the CSLDV signal with a scan frequency of 1Hz when the plate was driven at 106.9Hz and 277.7Hz. For mode 1 and mode 4, the sideband harmonics higher than the 14th and 32nd order, respectively, are in the noise of the signal, as seen in the power spectral density (PSD) plots in Figure 10a and 10b, and hence no harmonics above these orders were used when constructing the mode shapes. It is important to note that more than twice as many harmonics are needed to reconstruct a 2D shape when compared with the 1D line. For a 2D Lissajous curve like this, it becomes harder to take the time to check all of the harmonics in the signal or tell when they are or are not reasonable to include in the reconstructed shape.

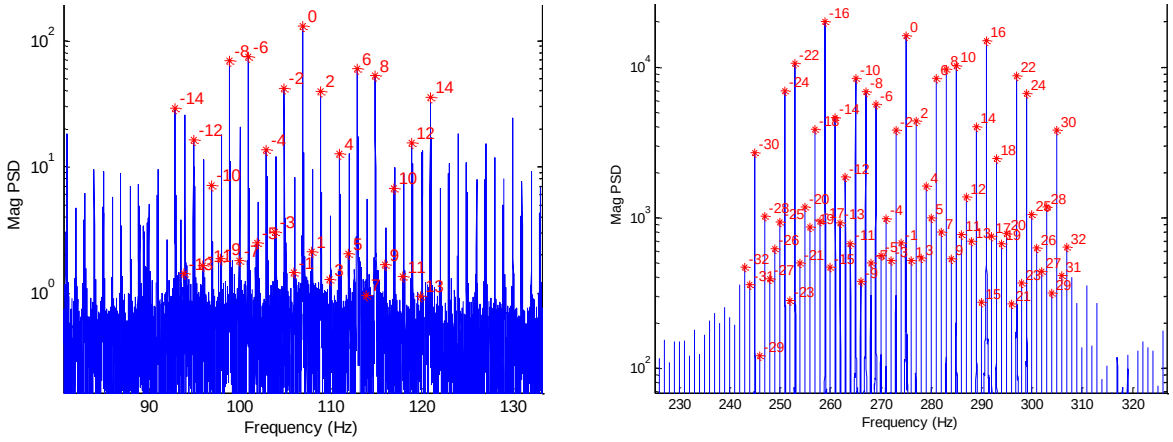

Figure 10: Power Spectra of CSLDV signals for a) mode 1 and b) mode 4

Figure 11 compares the mode shapes obtained by CSLDV and 3D-DIC for the two linear steady state experiments where the plate was excited with the magnetic driver. The shading describes the out of plane deformation of the plate as measured with both techniques. Figures 11a & 11b present the mode shape at 106.9Hz and show good agreement between both measurement techniques. Since there are no directly overlapping measurement points, MAC values cannot be calculated to compare the measured shapes, so only a qualitative comparison is made. The focus of this work was on modes of the plate

that would be excited with the use of symmetric loading (i.e. in the application of interest the aircraft panels are excited by uniform pressure loads), so the next linear mode examined was mode 4. Figures 11c & 11d contain the mode shape at 277.70 Hz and again show good agreement between measurements.

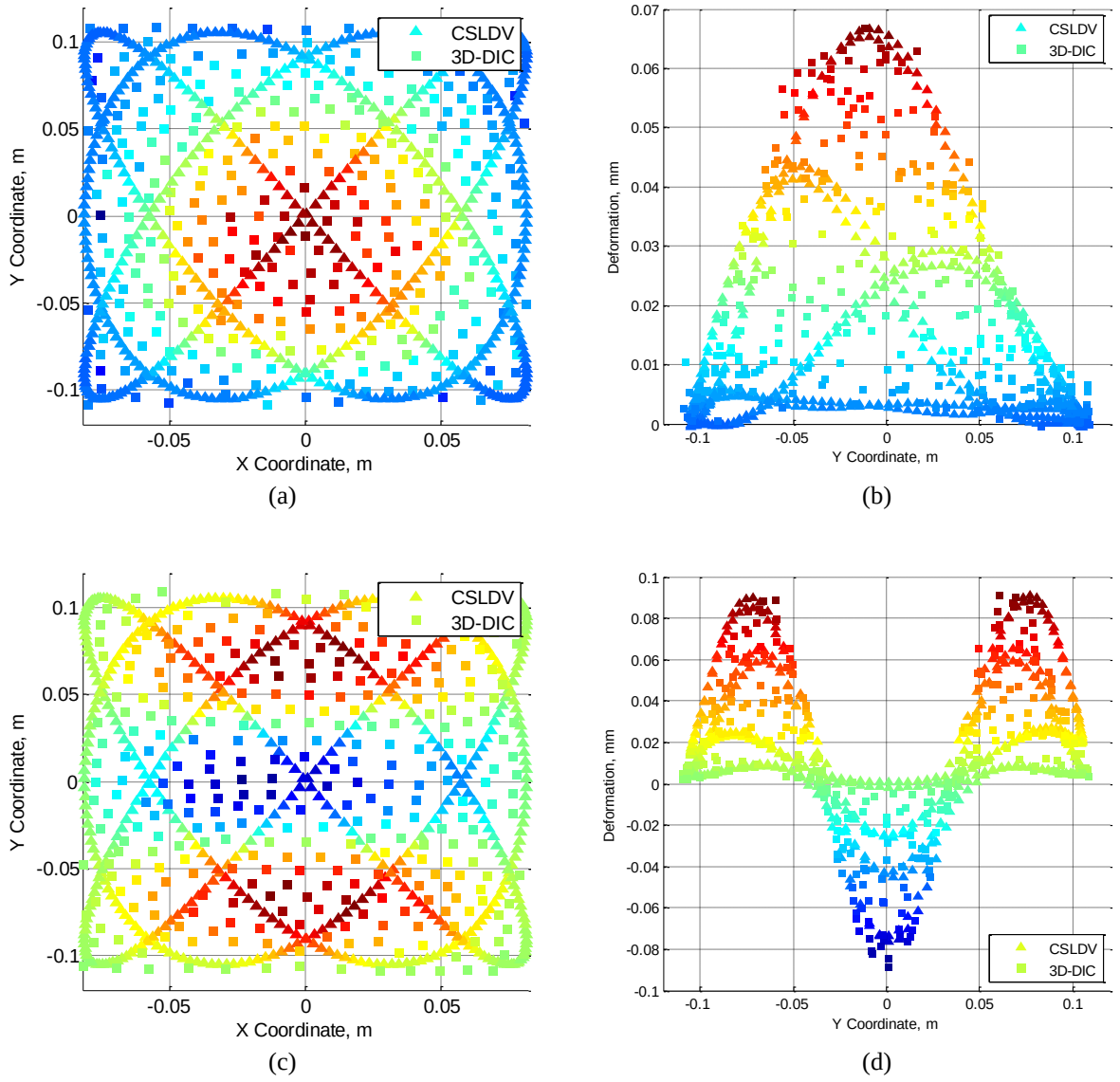

Figure 11: Mode Shape Comparison between CSLDV and 3D-DIC. a) & b) Mode 1, c) & d) Mode 4

5.2 Nonlinear Plate Response Comparison

Similar to the nonlinear excitation provided to the flat beam, the flat plate is excited at a large amplitude near the first resonant frequency. Since the plate is larger than the beam, a 5300 N shaker is used to provide base excitation to the flat plate. The deformation shapes at each harmonic are reconstructed with CSLDV using 32 sideband harmonics, the same

number that was used previously with the 4th linear mode shape. As is generally the case for a structure such as this [30], the primary harmonic of the measured nonlinear response, at 160.8Hz, resembles the first linear mode of the plate, as shown in Figure 12a and 12b. Both measurement systems capture this deformation well and are in good agreement with each other. The second harmonic of the nonlinear response, at 321.6Hz is shown in Figure 12c and 12d and was found to resemble the third linear mode of the plate. This deformation shape is unexpected since the base excitation that was used should theoretically not be able to directly excite an asymmetric mode such as this. Furthermore, the nonlinear normal modes [31] of a symmetric structure are typically all either purely symmetric or anti-symmetric [30, 32], so this measurement suggests that the asymmetry of the geometry of the plate is important to the nonlinear response and this information will be critical when modeling the structure. One should also note that asymmetric motions such as this are frequently observed in initially curved structures so the initial curvature of the plate should be modeled. Again, both measurement systems are able to capture this slightly more complicated mode shape.

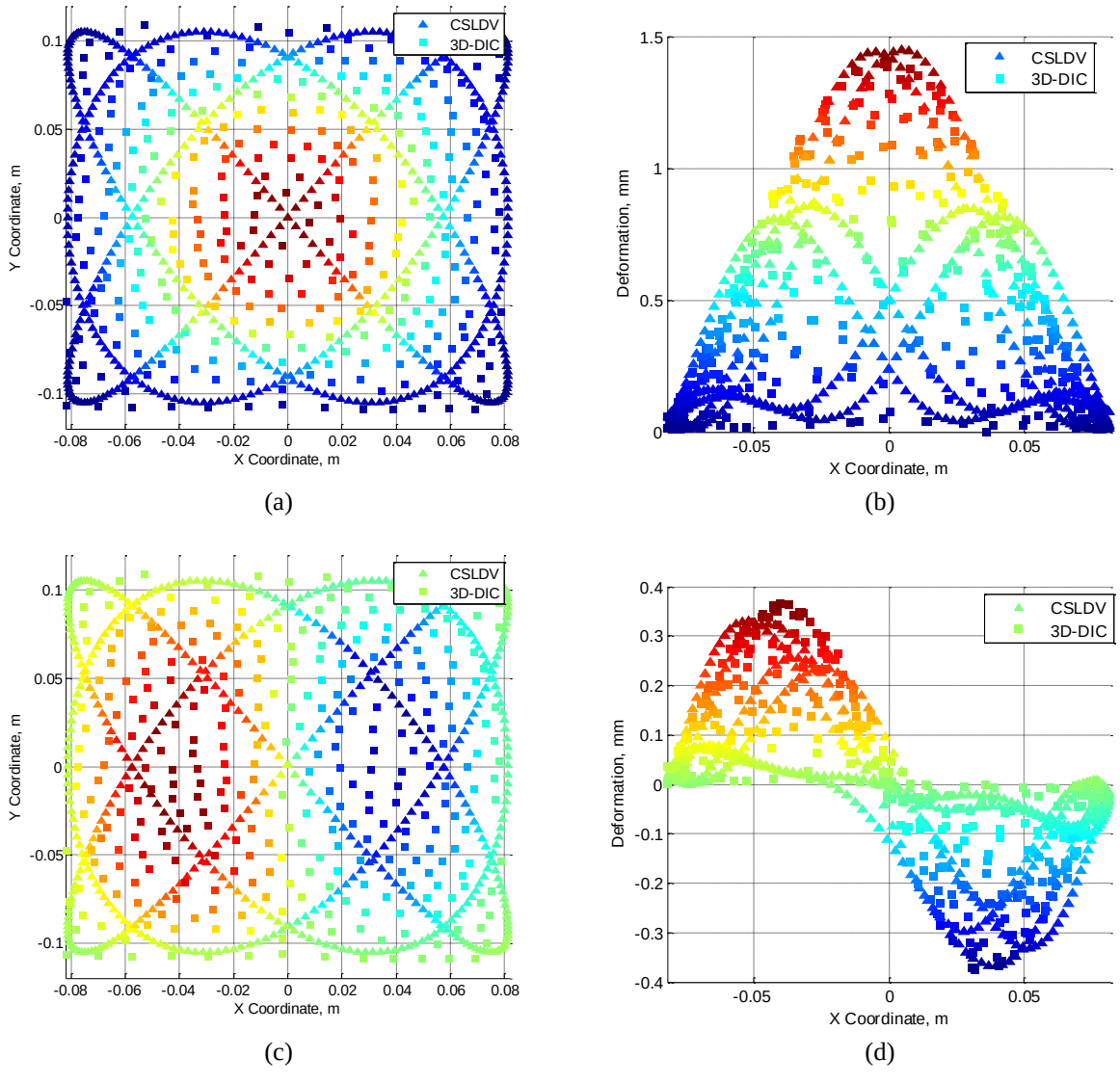

Figure 12: Deformation shape of CSLDV and 3D-DIC: a) & b) 1st harmonic, c) & d) 2nd harmonic

The third harmonic, at 482.4Hz, was found to resemble a rotated version of the 5th linear mode of the FEM as seen in Figure 13. This type of response is again unexpected as the characteristic shape is asymmetric in the y-coordinate. Again, both measurement systems capture the deformation shape well confirming the validity of this unexpected deformation shape. The fourth and the fifth harmonics showed similar results. The next harmonic examined is the sixth harmonic. Interestingly, the sixth harmonic's deformation shape, at 964.8Hz, resembles the 21st mode of the FE model. Here, the deformation shape is far more complicated, calling into question the accuracy of a CSLDV shape based on only 39 Fourier terms. The shape does not agree with itself at several of the points where the lines of the Lissajous figure cross. Additional terms could easily be added when post processing the measurement, but the sideband harmonics greater than 39 at the sixth harmonic do not stand out from the noise sufficiently to warrant adding additional terms. The accuracy of the deformation shape with 3D-DIC is also called into question since the deformation at this frequency is small, but the 3D-DIC measurement provides significantly better spatial resolution and that is helpful in understanding the shape.

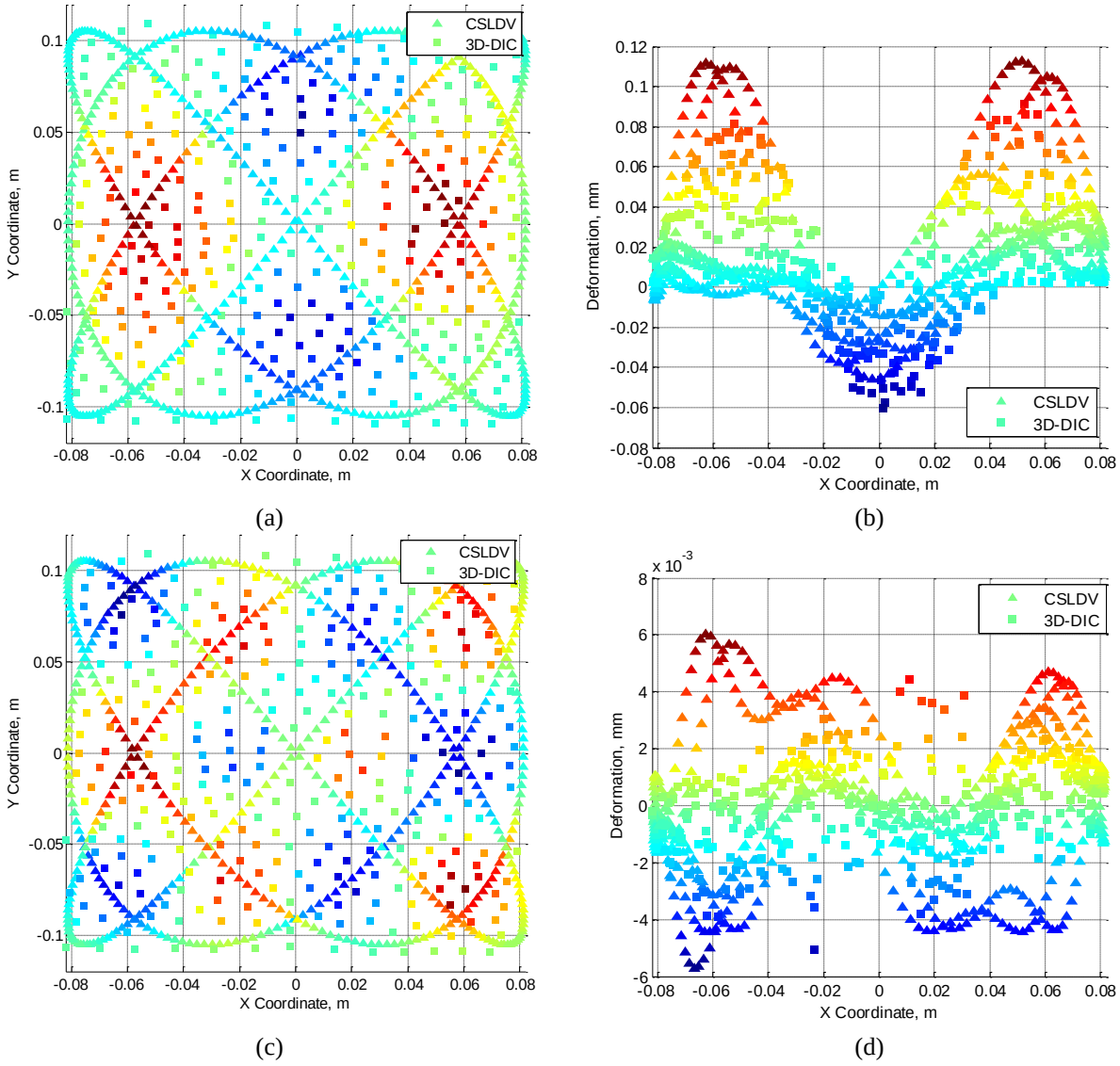

Figure 13: Deformation shape of CSLDV and 3D-DIC: a) & b) 3rd harmonic, c) & d) 6th harmonic

6. Conclusion

The mode shapes and natural frequencies of a clamped-clamped flat steel beam and a fully clamped rectangular aluminum plate were identified using CSLDV and high speed 3D-DIC. CSLDV was able to measure 1708 points across the surface of the beam and 10240 points across the surface of the plate. However, the information in the measurement is not governed by the number of points used to define the shape but by the number of Fourier coefficients that can be identified to describe the time-varying shape. In fact, decreasing the sample rate, and hence the number of sampled points, has sometimes been found to increase the resolution of the measurement [33]. The number of harmonics is especially important when a more complex 2-D measurement grid is used. Hence, the main disadvantage of CSLDV is that the harmonics describing the shapes are measured rather than the shapes at individual points, and so there may be uncertainty as to whether a feature in the measured deformation is really meaningful. On the other hand, CSLDV offers a few benefits over high-speed 3D-DIC: CSLDV can measure at large stand off distances, maintains accuracy over larger test specimens, and current LDVs clearly have much higher measurement resolution than DIC, down to tens of nano-meter/s velocities or pico-meter displacements. Some of that resolution can be lost to speckle noise when scanning the laser, and this was observed in the measurement of higher modes for the plate in this study, but even then CSLDV was shown to be more accurate than DIC when capturing the small amplitude linear of the beam and plate. For the (small-amplitude) higher harmonics of the nonlinear response the results were mixed; while CSLDV did have a lower noise floor the number of harmonics required to describe the motion increased significantly and in some cases accurate shapes still could not be measured. Finally, one should note that the quality of the CSLDV measurement depends on the type of laser, the surface quality, scanning frequency and other parameters so these observations will not hold for all structures.

High speed 3D-DIC was computed with 82 points for the beam and 300 points for the plate; however, a denser measurement grid could have been obtained if needed since the images were stored and post processed to obtain displacements. For the given field of view and geometry, 2500 points can be computed in a 2D grid across the surface of the beam and the measurement resolution is independent of measurement duration or excitation type. (In CSLDV, the spatial information is captured in empty regions between the excitation frequencies lines in the spectrum, and hence one must consider the input type, scan frequency, speckle noise, and the properties of the system to successfully capture measurements.) The spatial resolution of the acquired mode shape measured with high speed 3D-DIC is dependent on the stand off distance and the camera resolution; therefore, if more accurate measurements are needed, the camera setup needs to be moved closer to the test specimen, or a higher resolution camera is needed. Additionally, since high frequencies correspond to smaller displacements, high-speed 3D-DIC loses ability to measure mode shapes at higher frequencies. One

benefit high-speed 3D-DIC has over CSLDV is the ability to provide a 2D grid of measurement points equally spaced across the specimen surface that measures the three dimensional deformations providing near full-field measurements in all deformation axes, which were inconsequential for the flat structures investigated here. Indeed, with 3D-DIC one can capture the in-plane motions of the surface even more accurately than the out-of-plane motions, whereas CSLDV can only capture the motion along the axis of the incident laser beam.

Both techniques can provide dense measurements along surfaces, as long as each technique can "see" the surface. To provide accurate measurements, both techniques require surface preparation, unless the material used for the test piece fulfills specific requirements (e.g. a random pattern for 3D-DIC and a sufficiently reflective pattern for CSLDV). For DIC, this surface preparation is especially important when response levels are small, or in a structure's linear range. For CSLDV, surface preparation becomes more important when the vibration amplitude becomes small relative to speckle noise, and also as the laser standoff distance (or field of view) increases.

Finally, this study has illustrated that when full-field velocities or displacements are measured (i.e. as opposed to the usual case where the motion is only captured at a few points), inconsistencies in the dynamic behavior of the structure under test can be identified and provide insight to modeling and predicting dynamic behavior. Here, the CSLDV and DIC shapes revealed asymmetry in the 2nd and 3rd bending mode shapes of the beam and a skew in mode 1 of the bending mode shape of the plate, which was probably due to (un-modeled) asymmetry in the boundary conditions or initial geometry of the plate since it is thin. If a traditional test were performed with only a few measurement points, one would not be likely to detect this, nor would they have sufficient information to update the model to account for it.

Acknowledgements

Support for this research was provided by the University of Wisconsin – Madison Graduate School with funding from the Wisconsin Alumni Research Foundation and through the Structural Sciences Center in the Air Force Research Laboratory's summer internship program.

References

[1] A. B. Stanbridge and D. J. Ewins, "Modal Testing Using a Scanning Laser Doppler Vibrometer," *Mechanical Systems and Signal Processing*, vol. 13, pp. 255-270, 1999.

[2] A. B. Stanbridge, A. Z. Khan, and D. J. Ewins, "Modal testing using impact excitation and a scanning LDV," *Shock and Vibration*, vol. 7, pp. 91-100, 2000.

[3] M. Martarelli, "Exploiting the Laser Scanning Facility for Vibration Measurements," Ph.D. Ph.D. , Technology & Medice, Imperial College, London, 2001.

[4] A. B. Stanbridge, M. Martarelli, and D. J. Ewins, "Measuring area vibration mode shapes with a continuous-scan LDV," *Measurement*, vol. 35, pp. 181-189, 2004.

[5] C. W. Schwingshackl, A. B. Stanbridge, C. Zang, and D. J. Ewins, "Full-Field Vibration Measurement of Cylindrical Structures using a Continuous Scanning LDV Technique," presented at the 25th International Modal Analysis Confernce (IMAC XXV), Orlando, Florida, 2007.

[6] D. Di Maio, Ewins, D.J., "Continuous Scan, A Method for Performing Modal Testing Using Meaningful Measurement Parameters Part I," *Mechanical Systems and Signal Processing*, vol. 25, pp. 3024-42, 2011.

[7] M. S. Allen, "Frequency-Domain Identification of Linear Time-Periodic Systems Using LTI Techniques," *Journal of Computational and Nonlinear Dynamics*, vol. 4, pp. 041004-041004, 2009.

[8] S. Yang, M. W. Sracic, and M. S. Allen, "Two algorithms for mass normalizing mode shapes from impact excited continuous-scan laser Doppler vibrometry," *Journal of Vibration and Acoustics*, vol. 134, p. 021004, 2012.

[9] N. M. Wereley and S. R. Hall, "Frequency response of linear time periodic systems," in *Decision and Control, 1990., Proceedings of the 29th IEEE Conference on*, 1990, pp. 3650-3655 vol.6.

[10] N. M. Wereley, "Analysis and Control of Linear Periodically Time Varying Systems," Ph.D. Ph.D., Aeronautics and Astronautics, Massachusetts Institute of Technology, Cambridge, 1991.

[11] N. M. Wereley and S. R. Hall, "Linear Time Periodic Systems: Transfer Function, Poles, Transmission Zeroes and Directional Properties," in *American Control Conference, 1991*, 1991, pp. 1179-1184.

[12] S. Yang, and Allen, M.S., "Harmonic Transfer Function to Measure Translational and Rotational Velocities With Continuous-Scan Laser Doppler Vibrometry," *Journal of Vibration and Acoustics*, vol. 136, pp. 021025-021025, 2014.

[13] S. Yang, and Allen, M.S., "Output-Only Modal Analysis Using Continuous-Scan Laser Doppler Vibrometry and Application to a 20kW Wind Turbine," *Mechanical Systems and Signal Processing*, vol. 31, August 2012 2011.

[14] S. Yang, and Allen, M.S., "Lifting approach to simplify output-only continuous-scan laser vibrometry," *Mechanical Systems and Signal Processing*, vol. 45, pp. 267-282, 2014.

[15] T. E. Schmidt, J. Tyson, K. Galanulis, D. M. Revilock, and M. E. Melis, "Full-field dynamic deformation and strain measurements using high-speed digital cameras," in *26th International Congress on High-Speed Photography and Photonics*, Bellingham, WA, 2005, pp. 174-185.

[16] V. Tiwari, Sutton, M.A., Shultis, G., McNeill, S.R., Xu, S., Deng, X., Fourney, W.L., and Bretall, D., "Measuring full-field transient plate deformation using high speed imaging systems and 3D-DIC," in *Proceedings of the Society for Experimental Mechanics Annual Conference*, Albuquerque, 2009.

[17] C. Niezrecki, P. Avitabile, C. Warren, P. Pingle, and M. Helfrick, "A Review of Digital Image Correlation Applied to Structural Dynamics," *AIP Conference Proceedings*, vol. 1253, pp. 219-232, 2010.

[18] M. Helfrick, "3D Digital Image Correlation Methods for Full-Field Vibration Measurement," *Mechanical Systems and Signal Processing*, vol. 25, pp. 917-927, 2011.

[19] C. Warren, C. Niezrecki, P. Avitabile, and P. Pingle, "Comparison of FRF measurements and mode shapes determined using optically image based, laser, and accelerometer measurements," *Mechanical Systems and Signal Processing*, vol. 25, pp. 2191-2202, 2011.

[20] J. Abanto-Bueno, Ehrhardt, D., Shukla, A., and Parks, C., "Non-Contact Experimental Modal Analysis of a Curved Beam using a Full-Field Optical Technique," in *52nd AIAA/ASME/ASCE/AHS/ASC Structures, Structural Dynamics and Materials Conference*, ed: American Institute of Aeronautics and Astronautics, 2011.

[21] T. J. Beberniss, Spottswood, S.M., and Eason, T., "High-speed 3D digital image correlation measurement of long duration random vibration: recent advancements and noted limitaitons," presented at the ISMA Biennial Conference, Lueven, Belgium, 2012.

[22] D. A. Ehrhardt and T. J. Beberniss, "Experimental investigation of dynamic out of plane displacement error in 3D digital image correlation," in *54th AIAA/ASME/ASCE/AHS/ASC Structures, Structural Dynamics and Materials Conference, April 8, 2013 - April 11, 2013*, Boston, MA, United states, 2013.

[23] GOM, "Aramis," 6.3.0 ed. Braunschweig, Germany, 2011.

[24] GOM, "Real Time Sensor, IVIEW," 6.3.0 ed. Braunschweig, Germany, 2011.

[25] J. R. Bell, and Rothberg, S.J.,, "Laser Vibrometers and Contacting Transducers. Target Rotation and Six Degree-of-Freedom Vibration: What Do We Really Measure?," *Journal of Sound and Vibration*, vol. 237, pp. 245-261, 2000.

[26] M. A. Sutton, Orteu, J.J., and Schreier, H., *Image Correlation for Shape, Motion, and Deformation Measurements: Basic Concepts, Theory, and Applications*. New York, NY: Springer, 2009.

[27] R. W. Gordon, Hollkamp, J.J., and Spottswood, S. M., "Non-linear Response of a Clamped-Clamped Beam to Random Base Excitation," presented at the VIII International Conference on Recent Advances in Structural Dynamics, Southampton, United Kingdom, 2003.

[28] D. A. Ehrhardt, Yang, S., Beberniss, T.J., and Allen, M.S., "Mode Shape Comparison Using Continuous-Scan Laser Doppler Vibrometry and High Speed 3D Digital Image Correlation," presented at the International Modal Analysis Conference XXXII, Orlando, FL, 2014.

[29] R. W. Gordon, and Hollkamp, J.J., "Nonlinear Random Response of a Clamped Plate: A Well Characterized Experiment," *47th AIAA/ASME/ASCE/AHS/ASC Structures, Structural Dynamics, and Materials Conference*, vol. 6, pp. 4007-4024, 2006.

[30] R. J. Kuether and M. S. Allen, "A Numerical Approach to Directly Compute Nonlinear Normal Modes of Geometrically Nonlinear Finite Element Models," *Mechanical Systems and Signal Processing*, vol. 46, pp. 1–15, 2014.

[31] G. Kerschen, M. Peeters, J. C. Golinval, and A. F. Vakakis, "Nonlinear normal modes. Part I. A useful framework for the structural dynamicist," *Mechanical Systems and Signal Processing*, vol. 23, pp. 170-94, 2009.

[32] R. W. Gordon and J. J. Hollkamp, "Reduced-order Models for Acoustic Response Prediction," Air Force Research Laboratory, AFRL-RB-WP-TR-2011-3040, Dayton, OH2011.

[33] M. W. Sracic, and Allen, M.S., "Experimental Investigation of the Effect of Speckle Noise on Continuous Scan Laser Doppler Vibrometer Measurements," presented at the XXVII International Modal Analysis Conference, Orlando, FL, 2009.